Asian Journal of Chemistry; Vol. 38, No. 1 (2026), 133-140
ASIAN JOURNAL OF CHEMISTRY
https://doi.org/10.14233/ajchem.2026.34896

Synthesis of ZnSe Thin Films for Advanced Photodetector Applications: Impact of Deposition Time on Structural, Optical and Photoresponse Properties

NARAYAN M. NARKHEDE[1,2], V.S. BAVISKAR[2], S.R. GOSAVI[3], DEEPASHRI P. AHIRRAO[4] and PRAKASH B. AHIRRAO[1,*]

[1]Department of Physics, S.V.S.'s Dadasaheb Rawal College, Dondaicha-425408, India
[2]Department of Applied Science and Humanities, R.C. Patel Institute of Technology, Shirpur-425405, India
[3]Material Research Laboratory, C.H.C. Arts, S.G.P. Commerce and B.B.J.P. Science College, Taloda-425413, India
[4]Department of Physics, School of Physical Science, Kavayitri Bahinabai Chaudhari North Maharashtra University, Jalgaon-425001, India

*Corresponding author: E-mail: ahirraoprakash@gmail.com

Received: 15 September 2025 *Accepted*: 13 November 2025 *Published online*: 31 December 2025 AJC-22231

The present work investigates the simple and inexpensive chemical route for the fabrication of zinc selenide (ZnSe) nanocrystalline thin film for photosensing application. This study involved the systematic study of optical, structural, surface morphological characteristics as well as electron kinetics of the proposed ZnSe thin films with respect to the deposition time. The comprehensive analysis clearly revealed the formation of polycrystalline ZnSe thin film with enhancing the absorption of light in the visible region with respect to deposition time. Furthermore, the potential of the as-deposited ZnSe nanocrystalline thin film utilized for the photodetection in the visible region of the solar spectrum. The photodetection performance of the device was thoroughly analyzed through J-V characteristics, which clearly demonstrated that the performance of device is significantly influenced by the deposition time during chemical bath deposition. Optical analysis yielded similar results, with optical parameters such as optical conductivity and extinction coefficient exhibiting comparable trends. Remarkably, the device deposited for 3 h showed excellent photodetection performance, achieving detectivity and sensitivity value of 4.72×10^{11} Jones and 9.12, respectively.

Keywords: Zinc selenide, Chemical bath deposition, Thin films, Nanocrystalline, Photodetector.

INTRODUCTION

Rapid technological progress and the growing demand for efficient photovoltaic and optoelectronic devices underscore the need for continued materials research. Efforts should focus on identifying novel materials or improving existing ones by optimizing synthesis and post-treatment processes. Group I–VI compounds currently play a major role in these technologies due to their favourable physical and electronic properties, including wide band gaps, high transmittance and strong luminescence [1,2]. ZnSe has been gaining more and more interest among semiconductor chalcogenide, due to its enormous band gap of 2.71 eV at room temperatures [3], its abundant vibrant binding energy of (21 MeV) [4], minimal resistivity [5], strong luminescence efficiency [6] and remarkable photosensitivity [7] which make it a promising nominee for use in infrared detectors, photo-resistors, solar cells, optics, photovoltaics, photo-electronics and optoelectronics devices [8-13]. It is effectively utilized in thin transistors, laser screens [6], optically controlled switches, white light emitting diodes [14], dielectric mirrors and high infrared laser lenses [15]. Furthermore ZnSe is also thought to be a substitutional material employed as a buffer layer in the creation of highly effective solar cells using Cd-free thin films [16], since it is less hazardous and environmentally friendly [17].

In last decades, synthesis of ZnSe has been reported by using various depositions methods such as wet chemical method [18], thermal evaporation [19], sol-gel [20], pulsed laser deposition [21], solvothermal [22,23], atomic layer deposition [24], electrochemical deposition [25], spray pyrolysis [26], electrons beam evaporation [27], chemical vapour deposition (CVD) [28], solution growth techniques (SGT) [7], hydrothermal [29,30], successive ionic layer adsorption and reaction (SILAR) [31,32], photo-assisted chemical bath deposition (PCBD) [33]. Recently, another novel approach known as chemical bath deposition (CBD) has been employed for deposition ZnSe thin film in an aqueous solution [34-37].

The present research successfully demonstrates the use of nanocrystalline ZnSe thin films for photodetection applications. A simple and cost-effective chemical route, namely chemical bath deposition (CBD), was employed to prepare ZnSe thin films in an alkaline solution. The structural, optical, and surface morphological properties, along with the influence of deposition time on these characteristics, are systematically discussed. Finally, the photodetection potential of the FTO/ZnSe/Ag device is evaluated, and the effect of deposition time on the device-grade performance is comparatively analyzed.

EXPERIMENTAL

All chemicals used were of analytical reagent (AR) grade and did not require any further purification. Zinc sulphate hepta-hydrate ($ZnSO_4 \cdot 7H_2O$) (Merck), hydrazine hydrate (80%, N_2H_5OH), liquid ammonia, selenium powder (Se) (all from Loba chemie) and sodium sulphite (Na_2SO_3) (Merck) were used for the depositions of ZnSe thin films.

Substrate cleaning: A corning microscope fluorine-doped tin oxide (FTO)–coated conductive glass substrate with a sheet resistance of 15 Ω/cm^2 and an optical transmittance above 80% was employed for the deposition of nanocrystalline ZnSe thin films. This substrate was used to investigate the structural and optical characteristics of the films and to analyse their potential for photovoltaic performance. The FTO coated glass substrate were cleaned by using slandered process [38,39]. Initially, FTO coated glass substrate was cleaned in dilute HCl for 5 min, then ultrasonicated in soap solution for 15 min and rinsed in deionized water for 20 min. Without curing FTO coated glass film were further dipped in isopropyl alcohol for 10 min. Finally, the FTO coated glass films were rinsed well in deionized water and then kept in ultrasonic bath with deionized water for 15 min, dried in air and retain in an air-tight sealed container shortly before the deposition of the thin film.

Preparation of nanocrystalline ZnSe thin film: The facile chemical route employed in this work is the chemical bath deposition (CBD) technique, an advantageous method due to its simplicity, low cost and minimal instrumentation requirements. This technique was used for the growth of ZnSe nanoparticles on FTO-coated conductive glass substrates [40]. The incorporation of impurities is minimized in this method, making it more advantageous than other techniques. It enables the deposition of multi-component chalcogenide thin films across a broad stoichiometric range and offers high reproducibility.

In order to fabricate the nanocrystalline ZnSe thin films, zinc sulphate, selenium powder, sodium sulphite, hydrazine hydrate and liquid ammonia were taken as initial precursors. A freshly prepared 0.2 M $ZnSO_4$ solution was mixed with 1.3 mL of hydrazine hydrate and 1.8 mL of liquid NH_3, resulting in a pH of approximately 11 and served as Zn^{2+} ion source. The freshly prepared sodium selenosulphite (Na_2SeSO_3), as a source for Se^{2-} ions, was also prepared [40]. To prepare nanocrystalline ZnSe thin films, the positively charged and negatively charged precursors were combined in equal volumes in a beaker, the reaction bath was filled with 10 mL of 0.2 M $ZnSO_4$, 1.3 mL of hydrazine hydrate, 25% NH_4OH aqueous and 10 mL of freshly prepared Na_2SeSO_3 solution in a 25 mL beaker. Then, the FTO-coated conductive glass substrate was immersed in the beaker with its conductive surface facing the precursor solution. During deposition, hydrazine hydrate and ammonia acted as chelating agents, binding Zn^{2+} ions and controlling the precipitation rate for ZnSe film formation. Selenium ions (Se^{2-}) were supplied by sodium selenium sulphite. The deposition was carried out at 65 ºC for varying time period of 1, 2 and 3 h. After deposition, the substrates were removed, rinsed several times with deionized water to eliminate surface impurities and loosely bound species, and then air-dried. The resulting films exhibited a yellowish-red colour, adhered well to the substrate and were uniformly distributed across the surface.

Device fabrication: In order to build a device a silver (Ag) contacts was embedded on ZnSe thin film fabricated on the FTO decorated conductive glass by employing silver paste. A low-cost visible-light photodetector based on ZnSe was formed by applying silver contacts by using of Ag paste on ZnSe/FTO structure. In order to explore the photo-conductive and photo-detecting qualities, the device is light up by employing an incandescent lightbulb.

Characterization: The structural investigation of as-synthesized ZnSe thin film was studied with X-ray diffractometer (XRD) in the range of 20º to 80º. UV-Vis spectrophotometer (Shimadzu Models-1601) was employed to capture optical absorption spectra in the wavelength range of 300 to 800 nm. The surface morphological exploration was evidenced by the Hitachi S-4800 models of field emission scanning electron microscopy (FE-SEM). Energy dispersive X-rays spectroscopy (EDS) conjugation with FE-SEM instrument employed for the elemental compositional examination. The photovoltaic accurate measurements were performed in mimic sun light of intensity 100 mW/cm^2 using solar simulators (Tektronix, models Keithaly 4200A-SCS-PKA high resolutions IV).

RESULTS AND DISCUSSION

Structural studies: The structural properties of the as-synthesized ZnSe thin film were examined using X-ray diffraction (XRD) in the 2θ range of 20-80º for ZnSe thin films deposited *via* chemical bath deposition at different deposition times. Fig. 1 depicts the XRD peaks for as-synthesized ZnSe thin film with diffraction peak 2θ = 38.26º indexed to hexagonal crystal structure along with the (102) lattice plane (JCPDS card no. # 80-0008), which is expected to beneficial for photoconversion devices. Moreover, some minor peaks are also emerged at 29.33º, 45.70º, 49.68º, 56.55º and 60.51º, which are attributes to (101), (110), (103), (004) and (202) crystal planes, respectively indicating similar crystalline arrangements and phase. The appearance of fluorine doped tin oxide (FTO) has been proven by the extra diffraction peaks appeared at 26.40º, 43.06º and 51.56º with orientations along (221), (322) and (106) correspondingly [JCPDS card No. 82-2194]. The XRD findings have firmly confirm the fabrication of ZnSe thin film incorporated on FTO decorated glass substrate by CBD approach.

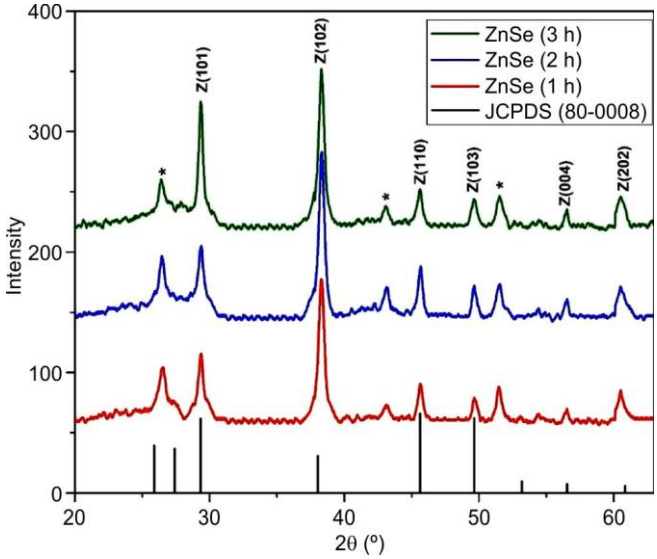

Fig. 1. X-ray diffraction patterns illustrating the crystallographic features of ZnSe for different deposition time

In particular, the size of crystallites (D) of ZnSe can be discover by applying Debye-Scherer's equations at an angle 38.26º.

$$D = \frac{k\lambda}{\beta \cos\theta} \quad (1)$$

where k is shape factor (0.9); λ is the wavelengths of X-rays (λ = 1.54056 Å); β is the full width at half of the peaks maximum in radians; and θ is the Bragg's angles. For as-deposited ZnSe the crystallite size was found to be ~86 nm.

Optical studies: The light harvesting ability of ZnSe tin films was incorporated by accruing optical absorption spectra in the 300 to 800 nm wavelengths region of the incident lights. Fig. 2a-b represent the typical optical transmittance and absorption spectra of ZnSe nanocrystalline thin films at 1 h, 2 h and 3 h deposition time. As depicted in Fig. 2a for all ZnSe samples, transmittance increases as a function of wavelength throughout the visible region and reaches an average values in the range from 20% to 58% for different deposition time. It is observed that the % transmittance decreases with increasing deposition time due to the formation of more nanostructured ZnSe films covering a larger portion of the substrate, resulting in thicker and more opaque films [6,41]. The absorption spectra of ZnSe thin films (Fig. 2b) show a significant enhancement in absorption in the lower wavelength (UV) region. These results suggest its potential as a window layer in solar conversion devices. Moreover, the increased light-harvesting ability in the visible range with longer deposition times is associated with enhanced generation of electron–hole pairs in the FTO/ZnSe structure, which is favourable for solar cell applications. The observed red shift in the absorption edge may be attributed to particle coalescence, where small nanoparticles aggregate into larger ones as deposition time increases during CBD. It is possible to obtain optical constant including absorption coefficient (α), extinction coefficient (k), refractive index (n) and optical conductivity (σ_{opt}) relating to materials by analysing transmission, absorbance and reflectance data [42]. A coefficient of absorption was computed by using eqn. 2 [43,44]:

$$\alpha = \frac{1}{d}\ln\left(\frac{1}{T}\right) \quad (2)$$

where the thickness (d) were obtain using cross-sectional analysis and found to be 510 nm, 691 nm and 832 nm for 1 h, 2 h and 3 h deposition time of ZnSe films, respectively. In addition, the absorption coefficients were used to determine a material's optical band gap (E_g). The optical band gap for ZnSe thin films sample of different deposition times has been estimated by extrapolating a linear portion of curve to a zero-absorption coefficient by using Tau plots as depicted in Fig. 3. Then, the optical band gap was estimated by extrapolating the linear portion of the absorption curve to zero absorption. The corresponding band gap values were found to be 2.86 eV, 2.67 eV and 2.50 eV for ZnSe films deposited for 1 h, 2 h, and 3 h, respectively. The observed shift in the optical band edge indicates the successful formation of nanocrystalline ZnSe thin films.

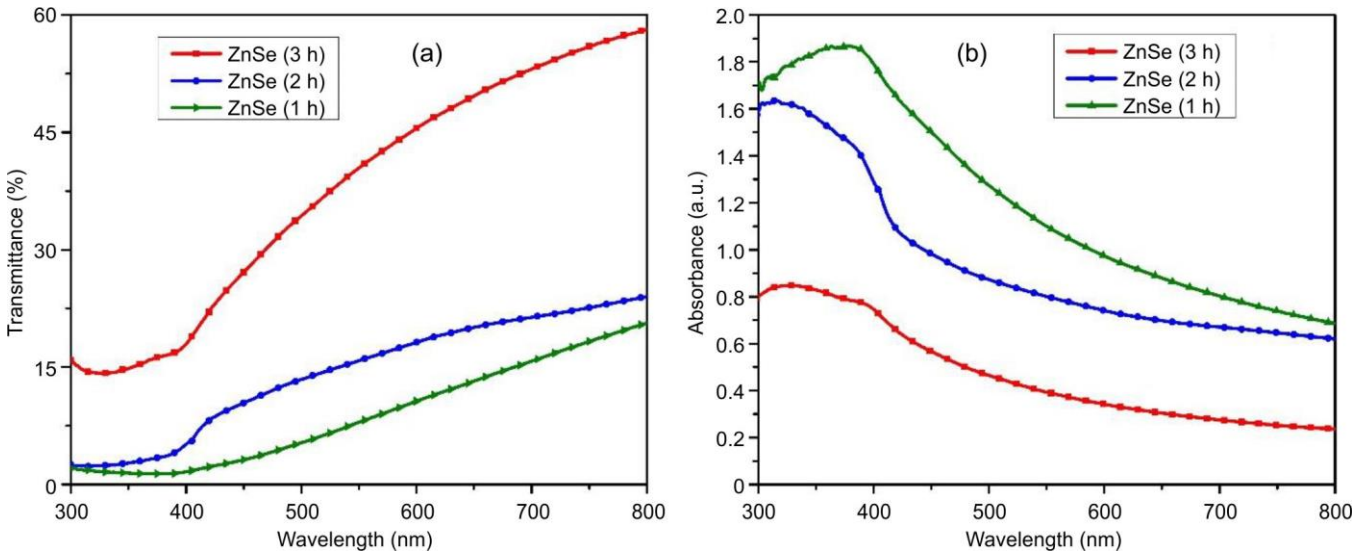

Fig. 2. (a) UV-Vis transmittance and (b) absorption spectra for ZnSe films for different deposition time

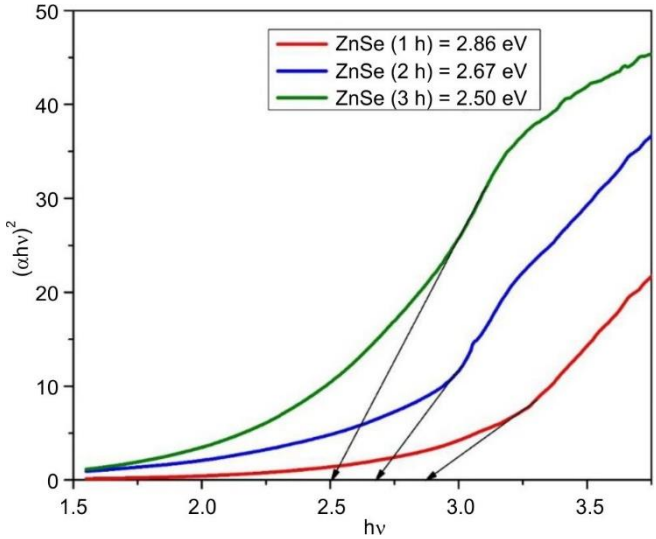

Fig. 3. Plots of $(\alpha h\nu)^2$ *versus* hν for ZnSe photoanodes of 1 h, 2 h and 3 h

The extinction coefficient (k), which quantifies the loss of light due to scattering and absorption, can be determined using eqn. 3 [41,45]:

$$k = \frac{\alpha\lambda}{4\pi} \quad (3)$$

The variation in magnitude of extinction coefficient (k) with variation in wavelength are shown in Fig. 4. The curve of the extinction coefficient shows a spectrum behaviour similar to that of absorbance. In other words, the observed absorption peaks indicate that the ZnSe films remain highly transparent in the 300-800 nm range, regardless of deposition time.

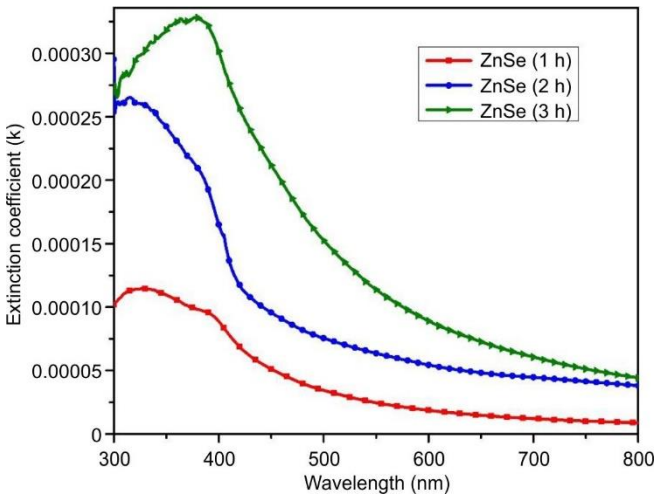

Fig. 4. The variation of extinction coefficients as a function of light wavelengths of ZnSe photoanodes of 1 h, 2 h and 3 h

For ZnSe films, the refractive index was calculated from the reflectance using eqn. 4 [46,47]:

$$n = \left(\frac{1+R}{1-R}\right) + \sqrt{\frac{4R}{(1-R)^2} - k^2} \quad (4)$$

where R retain the value for the reflectance. In order to calculate the reflectance, we use R = 1-T-A as a function of transmittance (T), reflection (R) and absorption (A) given by relation (A + T + R = 1) [48]. There are broad peaks in both the ultraviolet and visible regions in Fig. 5, due to the change in the refractive index with wavelength variation. This plot indicates that the refractive index of film is high in these regions. It is generally accepted that two fundamental optical properties refractive index (n) and extinction coefficient (K) are significant for optoelectronic devise [42].

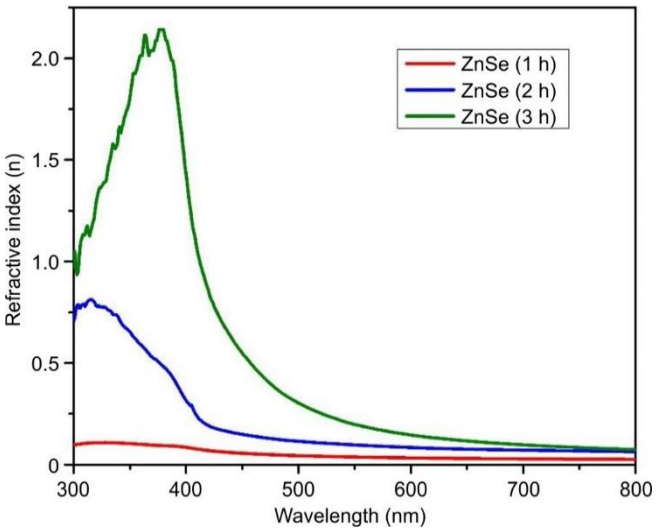

Fig. 5. The variation of refractive index as a function of light wavelengths of ZnSe photoanodes of 1 h, 2 h and 3 h

The key optical property namely optical conductivity (σ_{opt}) value corresponds to the interaction between light and materials and it can be calculated using refractive index and absorption coefficient as follows [49-51]:

$$\sigma_{opt} = \frac{\alpha nc}{4\pi} \quad (5)$$

where c represents the speed of light. The transformation in the values of optical conductivity (σ_{opt}) with photon energy increase are depicted in Fig. 6. Initially, σ_{opt} increases slowly up to approximately 2.8 eV, after which it rises rapidly due to the increasing number of free charge carriers with higher photon energy.

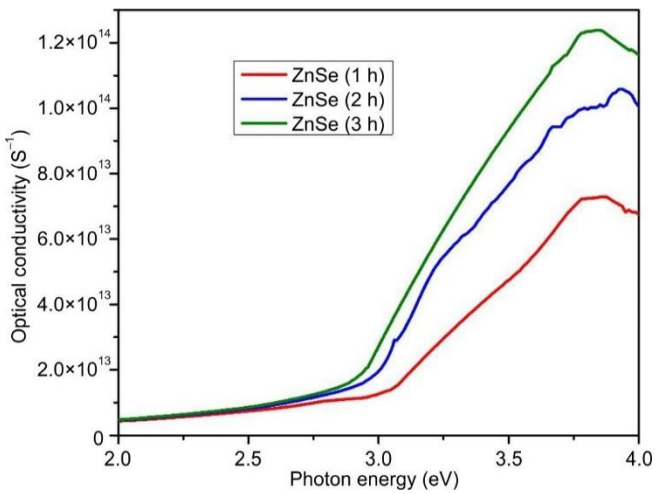

Fig. 6. The variation of optical conductivity as a function of photon energy of ZnSe photoanodes of 1 h, 2 h and 3 h

Surface morphology and compositional analysis: The morphological appearance of nanomaterials are significantly impacted by their physical and chemical characteristics. Fig. 7a-c revels the top view FE-SEM magnified visuals of ZnSe thin films deposited on the FTO decorated glass substrate at the indexing bar of 500 nm. Fig. 7a shows that ZnSe nanoparticles are evenly distributed on the substrate, promoting preferential nucleation. Increasing the deposition time from 1 h to 3 h allows pre-deposited ZnSe nanoparticles to serve as nucleation sites, facilitating secondary nucleation and further nanoparticle growth. This leads to agglomeration and increased bridging density on the FTO surface. Surface morphological analysis confirms that ZnSe nanoparticles were effectively deposited on FTO-coated glass at 65 ºC using the CBD method.

Elemental analysis was performed using energy-dispersive X-ray spectroscopy (EDS) coupled with FE-SEM operated at 20 kV, clearly showing peaks corresponding to Zn and Se, as illustrated in Fig. 7d. The EDS spectrum confirms the formation of a nanocrystalline ZnSe thin layer on the FTO surface. Overall, the EDS results strongly support the XRD findings, validating the successful fabrication of the FTO/ZnSe architecture *via* the proposed chemical bath deposition method.

Photovoltaic performance: The operation of the photodetector relies on transforming absorbed photons into an electrical signal. An in-depth comprehension of the basic functioning of the photodetector and its associated mechanisms is available in the existing literature [52,53]. In this study, the ZnSe film synthesized at different deposition time exhibits high crystallinity. Furthermore, the ZnSe films exhibit strong optical absorption in the visible region. Based on this, an Ag/ZnSe photodetector was fabricated on an FTO substrate using the FTO/ZnSe/Ag configuration.

Fig. 8 illustrates the schematic of the fabricated FTO/ZnSe photodetector device for the visible-light sensing capabilities at room temperature in both dark as well as illumination contexts. Due to high mobility, large band gap and appropriate band location with the current device structure make them a viable front contact and electron-transport layer (ETL).

The photoresponse of the FTO/ZnSe photodetectors was investigated under the both dark and white light exposure (100 mW cm^{-2}) at ambient temperature. Fig. 9 illustrates the current voltage (I-V) characteristics of the ZnSe-based photodetector in both dark and visible light illumination scenarios. The increase in the current value observed under white light

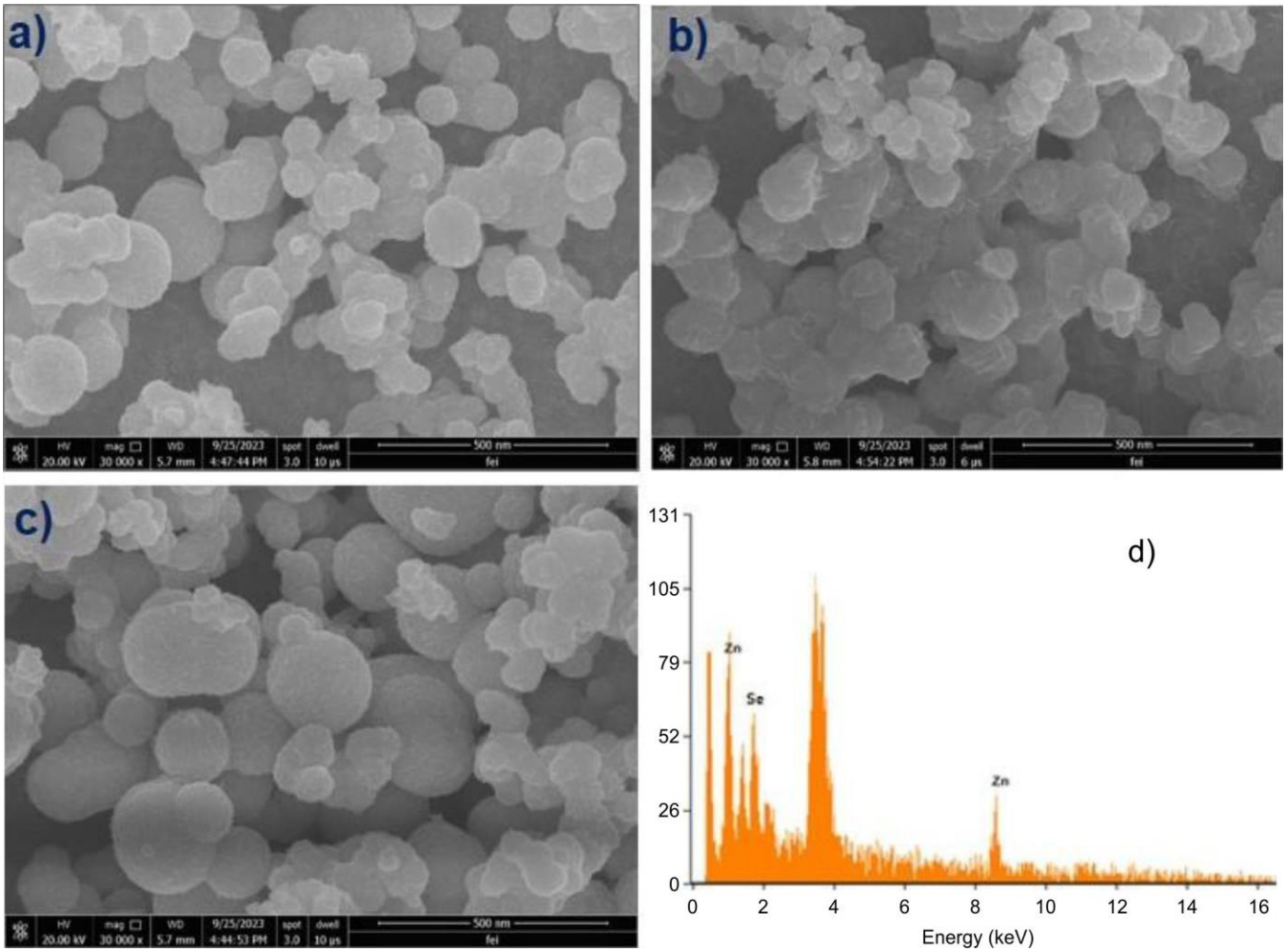

Fig. 7. Field emission scanning electron microscope images of (a) ZnSe (1 h), (b) ZnSe (2 h), (c) ZnSe (3 h) and (d) EDS spectrum of ZnSe (1 h)

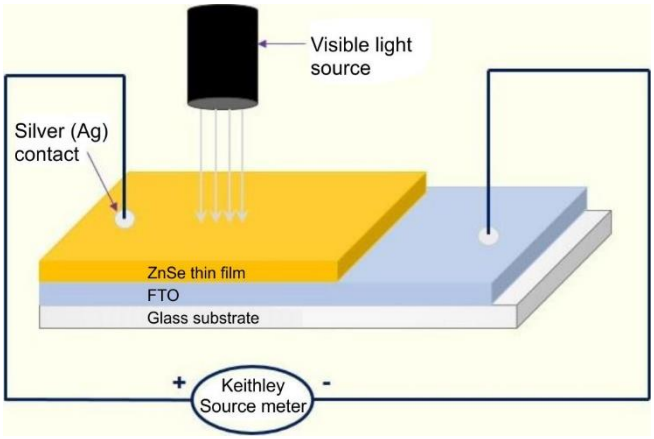

Fig. 8. Schematic depiction of FTO/ZnSe structure for visible light photodetector

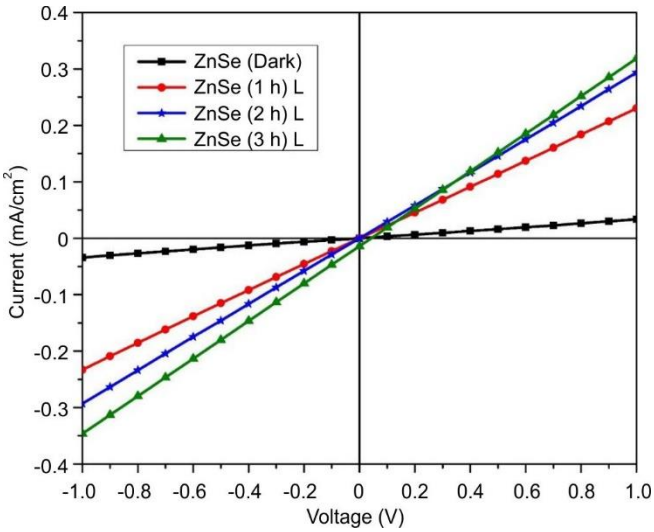

Fig. 9. Schematic representation of photocurrent density (J) *versus* photovoltage (V) characteristics curves of ZnSe photodetector for 1 h, 2 h and 3 h deposition time in dark and light

confirmed the semiconducting photoactive qualities of ZnSe with varying deposition times. Photodetectors typically function in a reverse-biased setup, utilizing reverse bias to expand the depletion region and improve photon absorption. In the forward bias range, which spans from 0 to 1 V, the I-V curve shows behaviour akin to that of a diode when the device is not illuminated.

However, when subjected to light, the photovoltaic effect drives the current into the fourth quadrant. This response to light is essential for the effective operation of the device as a photodetector. In contrast, a significant shift in the current value was observed in the reverse bias region (from -1 to 0 V) after the device was exposed to light, moving into the third quadrant. The performance of the ZnSe-based photodetector fabricated with varying deposition times, was examined by determining its photoresponsivity (R_λ), photosensitivity (ξ), external quantum efficiency (EQE) and detectivity (D*) factors. The photoresponsivity (R) has been described by the photocurrent obtained for each unit of light power density incident on the architecture and can be estimated by using eqn. 6:

$$R_\lambda = \frac{\Delta I}{P_{in} S} \quad (6)$$

where ΔI is the change in photocurrent due to incident light and is represented as $I_{photo} - I_{dark}$; P_{in} is the amount of intensity of the incident light; and S is the active surface area of the photodetectors. The calculated value of photoresponsivity for the ZnSe-based photodetector fabricated at different deposition time is listed in Table-1. The overall performance of the photodetector is greatly enhanced, as high crystallinity and larger crystallite size facilitate efficient transport of photogenerated electrons [54].

Photosensitivity (ξ) is a crucial parameter of a photodetector, defined as the change in current (ΔI) relative to the dark current, as expressed in eqn. 7 [55]:

$$\xi = \frac{I_{photo} - I_{dark}}{I_{dark}} \quad (7)$$

The external quantum efficiency (EQE) quantifies the efficiency of photodetector in converting photons into separated charge carriers [56]. It is expressed as the ratio of generated electrons or holes to the incident photons for a specified energy input [57] and represented as follows (eqn. 8):

$$EQE = R_\lambda \times \frac{h \times c}{q \times \lambda} \times 100 \quad (8)$$

where R_λ is photoresponsivity; h is Planck's constant; c is the speed of light; q is the absolute value of electron charge; and λ is the average wavelength of illuminated light.

Another crucial parameter known as detectivity (D*) measures the quality of the photodetector and is expressed as follows (eqn. 9):

$$D^* = \frac{R_\lambda \sqrt{S}}{\sqrt{2q \times J_{dark}}} \quad (9)$$

where J_{dark} represents the dark current density. The detectivity is measured in Jones and it helps to compare different photodetectors with different areas and geometries [58,59]. The computed values of photoresponsivity (R_λ), photosensitivity (ξ), external quantum efficiency (EQE) and detectivity (D*) of the ZnSe-based photodetector fabricated with varying deposition times are listed in Table-1.

TABLE-1
VALUES OF AVERAGE CRYSTALLITE SIZE, BAND GAP, PHOTORESPONSIVITY (R_λ), PHOTOSENSITIVITY (ξ), EXTERNAL QUANTUM EFFICIENCY (EQE) AND DETECTIVITY (D*) OF THE ZnSe-BASED PHOTODETECTOR FABRICATED WITH VARYING DEPOSITION TIMES

Deposition time (h)	D (nm)	Band gap	R_λ (μA W^{-1})	ξ	EQE (%)	D* (Jones)
ZnSe (1 h)	53.73	2.86	497.40	5.81	112.42	3.01×10^{11}
ZnSe (2 h)	54.08	2.67	647.40	7.56	146.33	3.91×10^{11}
ZnSe (3 h)	54.54	2.50	780.40	9.12	176.39	4.72×10^{11}

Conclusion

In this study, a highly efficient, stable and fast-switching ZnSe-based photodetector is fabricated using a simple and cost-effective chemical route. The optical, structural, surface morphological and electron transport properties of the ZnSe thin films were systematically examined with respect to the deposition time. Deposition time was found to have strong influences on these properties through the size tuning of ZnSe nanoparticles. Comparative analysis of device performance showed that the photodetector deposited for 3 h exhibited the highest photoresponsivity and photosensitivity of 780 μAW^{-1} and 9.12, respectively.

ACKNOWLEDGEMENTS

The authors express their heartfelt gratitude to the Principal and management of S.V.S.'s Dadasaheb Rawal College, Dondaicha for their kind assistance ship for this work. The authors also gratefully appreciated the help and lab facilities provided by Prof. J.V. Sali, School of Physical Science, Kavayitri Bahinabai Chaudhari North Maharashtra University, Jalgaon. Sincerely thanks are also extended to Dr. P.N. Patil, Dr. M.S. Sonawane, Dr. K.E. Suryawanshi, Dr. K.A. Isai, V.K. Suryanwanshi, Dr. H.S. Tarkas and Dr. P.V. Baviskar for their valuable support throughout this work.

CONFLICT OF INTEREST

The authors declare that there is no conflict of interests regarding the publication of this article.

DECLARATION OF AI-ASSISTED TECHNOLOGIES

During the preparation of this manuscript, the authors used an AI-assisted tool(s) to improve the language. The authors reviewed and edited the content and take full responsibility for the published work.

REFERENCES

1. R. Sharma, Himanshu, S.L. Patel, S. Chander, M.D. Kannan and M.S. Dhaka, *Phys. Lett. A*, **384**, 126097 (2020); https://doi.org/10.1016/j.physleta.2019.126097
2. N.S. Das, P.K. Ghosh, M.K. Mitra and K.K. Chattopadhyay, *Physica E*, **42**, 2097 (2010); https://doi.org/10.1016/j.physe.2010.03.035
3. F.M. Tezel and İ.A. Kariper, *Int. J. Mod. Phys. B*, **33**, 1950024 (2019); https://doi.org/10.1142/S0217979219500243
4. A. Salem, E. Saion, N.M. Al-Hada, H.M. Kamari, A.H. Shaari and S. Radiman, *Results Phys.*, **7**, 1175 (2017); https://doi.org/10.1016/j.rinp.2017.03.011
5. J. Sharma, D. Shikha and S.K. Tripathi, *Rom. Rep. Phys.*, **66**, 10002 (2014).
6. C. L. Li, K. Nishikawa, M. Ando, H. Enomoto and N. Murase, *Colloids Surf. A: Physicochem. Eng. Aspects*, **294**, 33 (2007); https://doi.org/10.1016/j.colsurfa.2006.07.052
7. H.K. Sadekar, A.V. Ghule and R. Sharma, *Compos., Part B Eng.*, **44**, 553 (2013); https://doi.org/10.1016/j.compositesb.2012.03.003
8. I.A. Kariper, *Surf. Rev. Lett.*, **27**, 1950128 (2019); https://doi.org/10.1142/S0218625X19501282
9. F. Aydın, F.M. Tezel and I.A. Kariper, *Mater. Res. Express*, **6**, 016425 (2018); https://doi.org/10.1088/2053-1591/aae9bf
10. F. Meydaneri Tezel and I.A. Kariper, *Mater. Res. Express*, **6**, 036412 (2018); https://doi.org/10.1088/2053-1591/aaf593
11. S. Sunaina, A.K. Ganguli and S.K. Mehta, *J. Alloys Comp.*, **894**, 162263 (2022); https://doi.org/10.1016/j.jallcom.2021.162263
12. N.A. Shah, M. Abbas, W. Adil and S.W. Mahmood, *Iran. J. Energy Environ.*, **5**, 87 (2014); https://doi.org/10.5829/idosi.ijee.2014.05.01.13
13. M. Imran, A. Saleem, N.A. Khan, A.A. Khurram and N. Mehmood, *Thin Solid Films*, **648**, 31 (2018); https://doi.org/10.1016/j.tsf.2018.01.010
14. C. Mehta, G.S.S. Saini, J.M. Abbas and S.K. Tripathi, *Appl. Surf. Sci*., **256**, 608 (2009); https://doi.org/10.1016/j.apsusc.2009.06.023
15. H.N. Desai, J.M. Dhimmar and B.P. Modi, *Mater. Today Proc*., **3**, 1650 (2016); https://doi.org/10.1016/j.matpr.2016.04.055
16. S.L. Deshmukh, P.C. Pingale, G.T. Chavan, S.T. Pawar, V.M. Prakshale, S.S. Kamble, S.R. Jadkar, N.B. Chaure, C.S. Gopinath, N.N. Maldar and L.P. Deshmukh, *J. Mater. Sci. Mater*. Electron., **28**, 5070 (2017); https://doi.org/10.1007/s10854-016-6144-3
17. R.B. Kale, C.D. Lokhande, R.S. Mane and S.-H. Han, *Appl. Surf. Sci*., **252**, 5768 (2006); https://doi.org/10.1016/j.apsusc.2005.07.063
18. M. Chen and L. Gao, *Mater. Chem. Phys*., **91**, 437 (2005); https://doi.org/10.1016/j.matchemphys.2004.12.005
19. A. Dahiya, S. Chuhadiya, D. Suthar, Himanshu, S.P. Nehra and M.S. Dhaka, *Physica B*, **645**, 414239 (2022); https://doi.org/10.1016/j.physb.2022.414239
20. A. Kaur and R. Kumar, *Asian J. Chem*., **29**, 1990 (2017); https://doi.org/10.14233/ajchem.2017.20712
21. D. Gao, L. Wang and X. Su, *Adv. Opt. Mater*., **11**, 2300311 (2023); https://doi.org/10.1002/adom.202300311
22. T. Gupta and R.P. Chauhan, *Surf. Interfaces*, **25**, 101196 (2021); https://doi.org/10.1016/j.surfin.2021.101196
23. X. Ren, Q. Li, Y. Xue, X. Zhai and M. Yu, *J. Colloid Interface Sci.*, **389**, 53 (2013); https://doi.org/10.1016/j.jcis.2012.08.052
24. M. Chazot, A. Kostogiannes, M. Julian, C. Feit, J. Sosa, M. Kang, C. Blanco, J. Cook, V. Rodriguez, F. Adamietz, D. Verreault, P. Banerjee, K. Schepler, M.C. Richardson and K.A. Richardson, *J. Non-Cryst. Solids*, **576**, 121259 (2022); https://doi.org/10.1016/j.jnoncrysol.2021.121259.
25. I.L. Ikhioya, C.O. Ugwuoke, D.N. Okoli, A.J. Ekpunobi, M. Maaza and F.I. Ezema, *Curr. Res. Green Sustain. Chem.*, **5**, 100328 (2022); https://doi.org/10.1016/j.crgsc.2022.100328
26. S.A. Suroor and H.S. Ali, *J. Opt*., **54**, 2814 (2025); https://doi.org/10.1007/s12596-024-02054-y
27. H.H. Gullu, M. Isik, N.M. Gasanly and M. Parlak, *Phys. Scr*., **95**, 075804 (2020); https://doi.org/10.1088/1402-4896/ab8eef
28. D. Li, N. Wei, J. Yang, C. Zhao, J. Zhou, J. Li and X. Liu, *Opt. Mater*., **132**, 112868 (2022); https://doi.org/10.1016/j.optmat.2022.112868
29. M.F. Ehsan, S. Bashir, S. Hamid, A. Zia, Y. Abbas, K. Umbreen, M.N. Ashiq and A. Shah, *Appl. Surf. Sci*., **459**, 194 (2018); https://doi.org/10.1016/j.apsusc.2018.07.162
30. D. Souri, N. Salimi and M. Ghabooli, *Inorg. Chem. Commun*., **123**, 108345 (2021); https://doi.org/10.1016/j.inoche.2020.108345
31. R.B. Kale and C.D. Lokhande, *Mater. Res. Bull*., **39**, 1829 (2004); https://doi.org/10.1016/j.materresbull.2004.06.014
32. P.M. Geethanjali, K. Deepa and T.L. Remadevi, *AIP Conf. Proc*., **2352**, 020011 (2021); https://doi.org/10.1063/5.0052381
33. D.D. Hile, H.C. Swart, S.V. Motloung, R.E. Kroon, K.O. Egbo and L.F. Koao, *J. Phys. Chem. Solids*, **140**, 109381 (2020); https://doi.org/10.1016/j.jpcs.2020.109381
34. G. Bakiyaraj and R. Dhanasekaran, *Appl. Nanosci*., **3**, 125 (2013); https://doi.org/10.1007/s13204-012-0075-y

35. R. Khalfi, D. Talantikite-Touati, A. Tounsi and H. Merzouk, *Opt. Mater.*, **106**, 109989 (2020); https://doi.org/10.1016/j.optmat.2020.109989
36. S. Sagadevan and I. Das, *Aust. J. Mech. Eng.*, **15**, 222 (2017); https://doi.org/10.1080/14484846.2016.1264347
37. G.L. Agawane, S.W. Shin, M.P. Suryawanshi, K.V. Gurav, A.V. Moholkar, J.Y. Lee, P.S. Patil, J.H. Yun and J.H. Kim, *Ceram. Int.*, **40A**, 367 (2014); https://doi.org/10.1016/j.ceramint.2013.06.011
38. S.V. Baviskar, D.B. Salunkhe, C.P. Nikam, N.M. Narkhede, C.D. Jadhav, G.P. Patil and R.S. Patil, *Nano-Struct. Nano-Objects*, **32**, 100919 (2022); https://doi.org/10.1016/j.nanoso.2022.100919
39. S.V. Baviskar, C.D. Jadhav, D.B. Salunkhe, N.M. Narkhede and G.P. Patil, *Next Energy*, **6**, 100190 (2025); https://doi.org/10.1016/j.nxener.2024.100190
40. N.M. Narkhede, V.S. Baviskar, H.S. Tarkas and P.B. Ahirrao, *Int. J. Innov. Res. Technol.*, **11**, 37 (2025).
41. C. Emir, A. Tataroglu, U. Gokmen and S.B. Ocak, *J. Mater. Sci. Mater. Electron.*, **36**, 168 (2025); https://doi.org/10.1007/s10854-025-14221-3
42. J. Tauc, *Mater. Res. Bull.*, **3**, 37 (1968); https://doi.org/10.1016/0025-5408(68)90023-8
43. O. Gullu and A. Tataroglu, *Opt. Mater.*, **148**, 114881 (2024); https://doi.org/10.1016/j.optmat.2024.114881
44. S. Thirumavalavan, K. Mani and S. Sagadevan, *Mater. Today Proc.*, **3**, 2305 (2016); https://doi.org/10.1016/j.matpr.2016.04.141
45. H.I. Elsaeedy, A.A. Hassan, H.A. Yakout and A. Qasem, *Opt. Laser Technol.*, **141**, 107139 (2021); https://doi.org/10.1016/j.optlastec.2021.107139
46. H. Qi, X. Zhang, M. Jiang, Q. Wang and D. Li, *J. Appl. Spectrosc.*, **84**, 679 (2017); https://doi.org/10.1007/s10812-017-0529-9
47. A.M. Bolbol, O.H. Abd-Elkader, H. Elshimy, Z.I. Zaki, S.A. Shata, M. Kamel, A.S. Radwan and N.Y. Mostafa, *Results Phys.*, **42**, 105955 (2022); https://doi.org/10.1016/j.rinp.2022.105955
48. M.F. Rahman, J. Hossain and A.B.M. Ismail, *SN Appl. Sci.*, **2**, 1956 (2020); https://doi.org/10.1007/s42452-020-03836-2
49. V. Dhanasekaran, T. Mahalingam, J.-K. Rhee and J.P. Chu, *Optik*, **124**, 255 (2013); https://doi.org/10.1016/j.ijleo.2011.11.063
50. A. Salhi, S. Sayouri and M. Haddad, *Opt. Mater.*, **133**, 113008 (2022); https://doi.org/10.1016/j.optmat.2022.113008
51. S. Mondal, S. Sen, A. Kumar and H. Mudila, *Results Opt.*, **13**, 100556 (2023); https://doi.org/10.1016/j.rio.2023.100556
52. H. Tarkas, A. Rokade, D. Upasani, N. Pardhi, A. Rokade, J. Sali, S.P. Patole and S. Jadkar, *RSC Adv.*, **14**, 4352 (2024); https://doi.org/10.1039/D3RA07679B
53. H. Tarkas, A. Rokade, D. Upasani, J. Sali, V. Waman, A. Rokade and S. Jadkar, *New J. Chem.*, **48**, 4456 (2024); https://doi.org/10.1039/D4NJ00075G
54. P.S. Shewale and Y.S. Yu, *J. Alloys Compd.*, **654**, 79 (2016); https://doi.org/10.1016/j.jallcom.2015.09.048
55. D. Mottram, Y.H. Lin, P. Pattanasattayavong, K. Zhao, A. Amassian and T.D. Anthopoulos, *ACS Appl. Mater. Interfaces*, **8**, 4894 (2016); https://doi.org/10.1021/acsami.5b11210
56. B. Ezhilmaran, A. Patra, S. Benny, M.R. Sreelakshmi, V.V. Akshay, S.V. Bhat and C.S. Rout, *J. Mater. Chem. C Mater. Opt. Electron. Devices*, **9**, 6122 (2021); https://doi.org/10.1039/D1TC00949D
57. N. Huo and G. Konstantatos, *Adv. Mater.*, **30**, 1801164 (2018); https://doi.org/10.1002/adma.201801164
58. P.H. Chang, C.S. Li, F.Y. Fu, K.Y. Huang, A.S. Chou and C.I. Wu, *Adv. Funct. Mater.*, **28**, 1800179 (2018); https://doi.org/10.1002/adfm.201800179
59. Y. Wang, R. Fullon, M. Acerce, C.E. Petoukhoff, J. Yang, C. Chen, S. Du, S.K. Lai, S.P. Lau, D. Voiry, D. O'Carroll, G. Gupta, A.D. Mohite, S. Zhang, H. Zhou and M. Chhowalla, *Adv. Mater.*, **29**, 1603995 (2017); https://doi.org/10.1002/adma.201603995